Results in Physics 58 (2024) 107515

Contents lists available at ScienceDirect

Results in Physics

journal homepage: www.elsevier.com/locate/rinp

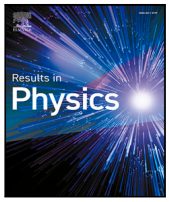

Optical microscale for antiferromagnetic $Sv-$ optimistic conformable density

Ferdous M. Tawfig [a], Talat Körpinar [b], Zeliha Körpinar [c], Mustafa Inc [d,e,*]

[a] Department of Mathematics, King Saud University, Riyadh 11495, Saudi Arabia
[b] Department of Mathematics, Muş Alparslan University, 49250, Muş, Turkey
[c] Department of Administration, Muş Alparslan University, 49250, Muş, Turkey
[d] Department of Mathematics, Fırat University, 23119, Elazığ, Turkey
[e] Department of Medical Research, China Medical University, 40402 Taichung, Taiwan

ARTICLE INFO

Keywords:
Optical antiferromagnetic model
Conformable deSitter space
Microfluidic microscale
Optimistic density

ABSTRACT

In this paper, we present spherical antiferromagnetic $Sv-$ magnetic electromotive conformable $\Phi(\tau),\Phi(\nu),\Phi(\beta)$ microscales in conformable deSitter space. Also, we get optical antiferromagnetic $Sv-$optimistic conformable $\Phi(\tau),\Phi(\nu),\Phi(\beta)$ densities. Finally, we obtain geometric antiferromagnetic $Sv-$magnetic conformable $\Phi(\tau),\Phi(\nu),\Phi(\beta)$ microscales in conformable deSitter space.

Introduction

The modeling of optical electric and magnetic phases presents an essential role in optical physics, optical design of a wide range of optical components and devices with quantum applications in fields such as flux, imaging, and quantum electronic components. The investigation of geometric microfluidics phases constructs complex optical random systems [1–20].

Optical electromagnetic phase and flux are applied within specific geometric generation frameworks. The modeling of hybrid electromagnetic phases of antiferromagnetic and Heisenberg ferromagnetic effects have applications in complex electromagnetic flux and fluid dynamics with electromotive microscale systems [21–37].

The microscale model of ferromagnetic phases with electromagnetism in ferrophases for optical applications are important research model in materials shape, optical physics, and modeling. This model has important potential to drive energy flux in various optical fields, from electronics to energy conversion and flexible phases. Electromagnetic properties of ferrophases are significant in various optical geometric applications [38–56].

Optical applications of microscale structures offer a wide range of possibilities for various fields, including materials science, biotechnology, electronics, cell sorting, micromanipulation, and biophysics research. Electromotive microscale structures are combined into microfluidic designs to manipulate fluids on complex random models [57–67].

Research on spherical antiferromagnetic $Sv-$ magnetic electromotive is currently quite poor. In our study, we created optical antiferromagnetic $Sv-$optimistic conformable density for the first time. The aim of our work, a general development method, is recommended for spherical optimistic density of conformable flow equations with illustrations of results in deSitter space. We view the cases of electromagnetic antiferromagnetic model for Lorentz forces. The advantage of our used deSitter space is spherical Minkowski space. Thus, we easily obtain spherical conformable flows in deSitter space [68,69]. The applications of antiferromagnetic model are electromagnetic surfaces [70–74].

The establishment of our paper is as follows. First, we characterize spherical antiferromagnetic $Sv-$magnetic electromotive conformable $\Phi(\tau),\Phi(\nu),\Phi(\beta)$ microscales in conformable deSitter space. Also, we get optical antiferromagnetic $Sv-$optimistic conformable $\Phi(\tau),\Phi(\nu),\Phi(\beta)$ densities. Finally, we obtain geometric antiferromagnetic $Sv-$ magnetic conformable $\Phi(\tau),\Phi(\nu),\Phi(\beta)$ microscales in conformable deSitter space.

Optical recursional operator

Considering conformable derivative model of spherical conformable frame $\{\tau,\nu,\beta\}$ is

$$\partial_\sigma \tau = \epsilon^{-\sigma+1}\nu,$$
$$\partial_\sigma \nu = \epsilon^{-\sigma+1}\tau + \epsilon^{1-\sigma}\mu\beta,$$

* Corresponding author.
E-mail addresses: ftoufic@ksu.edu.sa (F.M. Tawfig), talatkorpinar@gmail.com (T. Körpinar), zelihakorpinar@gmail.com (Z. Körpinar), minc@firat.edu.tr (M. Inc).

https://doi.org/10.1016/j.rinp.2024.107515
Received 14 September 2023; Received in revised form 10 February 2024; Accepted 23 February 2024
Available online 27 February 2024
2211-3797/© 2024 The Authors. Published by Elsevier B.V. This is an open access article under the CC BY-NC license (http://creativecommons.org/licenses/by-nc/4.0/).

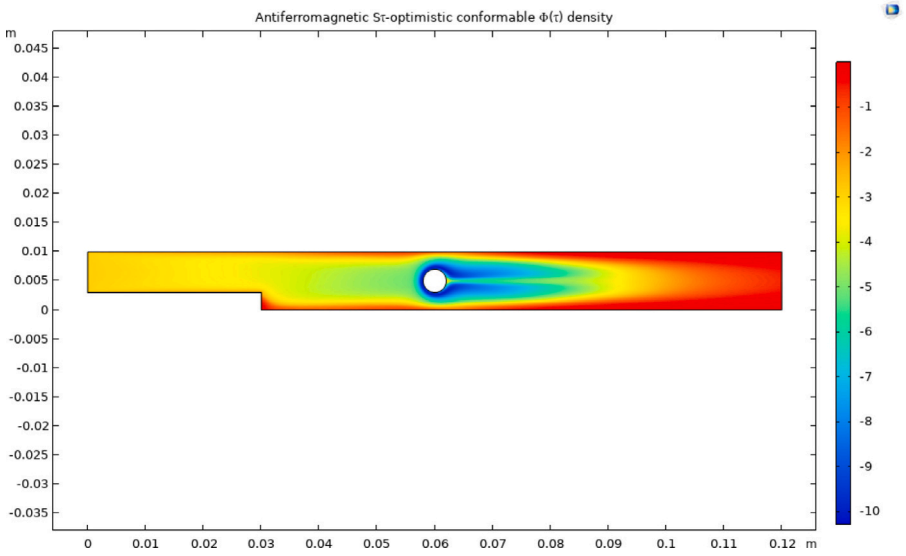

Fig. 1. $Sv-$ optimistic conformable $\Phi(\tau)$ density with reactor at $300K$.

$\partial_\sigma \beta = \mu\epsilon^{1-\sigma}\nu.$

Also field products given by

$\tau \times \beta = \nu,$

$\nu \times \beta = \tau,$

$\tau \times \nu = \beta,$

$\langle \tau,\tau \rangle = 1,\ \langle \nu,\nu \rangle = -1,\ \langle \beta,\beta \rangle = 1.$

‡ *Lorentz $\nu-$conformable fields are given*

$\Phi(\tau) = \epsilon^{1-\sigma}\nu + \varkappa\beta,$

$\Phi(\nu) = \epsilon^{1-\sigma}\tau + \epsilon^{1-\sigma}\mu\beta,$

$\Phi(\beta) = -\varkappa\tau + \mu\epsilon^{1-\sigma}\nu,$

$\mathbf{G} = \mu\epsilon^{1-\sigma}\tau - \varkappa\nu - \epsilon^{1-\sigma}\beta,$

where $\varkappa = g(\Phi(\tau), \beta)$ is conformable smooth potential.

Since, we have

$\partial_\sigma \Phi(\tau) = \epsilon^{2-2\sigma}\tau + (\varkappa\epsilon^{1-\sigma}\mu + \epsilon^{1-2\sigma}(1-\sigma))\nu + (\epsilon^{2-2\sigma}\mu + \epsilon^{1-\sigma}\frac{\partial\varkappa}{\partial\epsilon})\beta,$

$\partial_\sigma \Phi(\nu) = \epsilon^{1-2\sigma}(1-\sigma)\tau + (\epsilon^{2-2\sigma}\mu^2 + \epsilon^{2-2\sigma})\nu + (\mu(1-\sigma)\epsilon^{-2\sigma+1} + \frac{\partial\mu}{\partial\epsilon}\epsilon^{2-2\sigma})\beta,$

$\partial_\sigma \Phi(\beta) = (-\frac{\partial\varkappa}{\partial\epsilon}\epsilon^{1-\sigma} + \epsilon^{2-2\sigma}\mu)\tau + (\epsilon^{2-2\sigma}\frac{\partial\mu}{\partial\epsilon} + (1-\sigma)\epsilon^{1-2\sigma}\mu - \epsilon^{1-\sigma}\varkappa)\nu + (\mu\epsilon^{1-\sigma})^2\beta.$

$Sv-$Electromotive conformable $\Phi(\tau)$ microscale

First, we can represent by

$\Phi(\tau) = \epsilon^{1-\sigma}\nu + \varkappa\beta$

By conformal differentiating above field, we get

$\partial_\sigma \Phi(\tau) = \epsilon^{2-2\sigma}\tau + (\varkappa\epsilon^{1-\sigma}\mu + \epsilon^{1-2\sigma}(1-\sigma))\nu + (\epsilon^{2-2\sigma}\mu + \epsilon^{1-\sigma}\frac{\partial\varkappa}{\partial\epsilon})\beta.$

Therefore, we can write

$\Phi(\tau) \times \partial_\sigma \Phi(\tau) = (\epsilon^{1-\sigma}(\epsilon^{2-2\sigma}\mu + \epsilon^{1-\sigma}\frac{\partial\varkappa}{\partial\epsilon}) - \varkappa(\varkappa\epsilon^{1-\sigma}\mu + \epsilon^{1-2\sigma}(1-\sigma)))\tau - \varkappa\epsilon^{2-2\sigma}\nu - \epsilon^{3-3\sigma}\beta.$

The flow of $\Phi(\tau)$ is written by

$\partial_t \Phi(\tau) = (\epsilon^{2-2\sigma}\mathcal{F} - \mathcal{L}\varkappa\epsilon^{1-\sigma})\tau + (\varkappa(\epsilon^{1-\sigma}\frac{\partial\mathcal{L}}{\partial\epsilon} + \mathcal{F}\epsilon^{1-\sigma}\mu))\nu + (\frac{\partial\varkappa}{\partial t} + \epsilon^{1-\sigma}(\frac{\partial\mathcal{L}}{\partial\epsilon}\epsilon^{1-\sigma} + \mathcal{F}\epsilon^{1-\sigma}\mu))\beta.$

♣ *Optical $Sv-$magnetic electromotive conformable $\Phi(\tau)$ microscale is presented*

$\mathcal{E}_{\Phi(\tau)} = -\frac{d}{dt}\int_\tau \mathbb{I}_\sigma(\varkappa(\varkappa(\epsilon^{1-\sigma}\frac{\partial\mathcal{L}}{\partial\epsilon} + \mathcal{F}\epsilon^{1-\sigma}\mu)) + \mu\epsilon^{1-\sigma}(\epsilon^{2-2\sigma}\mathcal{F} - \mathcal{L}\varkappa\epsilon^{1-\sigma}) + \epsilon^{1-\sigma}(\frac{\partial\varkappa}{\partial t} + \epsilon^{1-\sigma}(\frac{\partial\mathcal{L}}{\partial\epsilon}\epsilon^{1-\sigma} + \mathcal{F}\epsilon^{1-\sigma}\mu)))d\pi.$

♣ *Optical $Sv-$optimistic conformable $\Phi(\tau)$ density is*

$\mathcal{D}_{\Phi(\tau)} = \mu\epsilon^{1-\sigma}(\epsilon^{2-2\sigma}\mathcal{F} - \mathcal{L}\varkappa\epsilon^{1-\sigma}) + \varkappa(\varkappa(\epsilon^{1-\sigma}\frac{\partial\mathcal{L}}{\partial\epsilon} + \mathcal{F}\epsilon^{1-\sigma}\mu)) + \epsilon^{1-\sigma}(\frac{\partial\varkappa}{\partial t} + \epsilon^{1-\sigma}(\frac{\partial\mathcal{L}}{\partial\epsilon}\epsilon^{1-\sigma} + \mathcal{F}\epsilon^{1-\sigma}\mu))$

♣ *Geometric $Sv-$magnetic conformable $\Phi(\tau)$ microscale is presented by*

${}^{B}\mathcal{M}_{\Phi(\tau)} = \epsilon^{1-\sigma}\varepsilon\int_\tau \mathbb{I}_\sigma(\epsilon^{1-\sigma}(\frac{\partial\varkappa}{\partial t} + \epsilon^{1-\sigma}(\frac{\partial\mathcal{L}}{\partial\epsilon}\epsilon^{1-\sigma} + \mathcal{F}\epsilon^{1-\sigma}\mu)) + \mu\epsilon^{1-\sigma}(\epsilon^{2-2\sigma}\mathcal{F} - \mathcal{L}\varkappa\epsilon^{1-\sigma}) + \varkappa(\varkappa(\epsilon^{1-\sigma}\frac{\partial\mathcal{L}}{\partial\epsilon} + \mathcal{F}\epsilon^{1-\sigma}\mu)))d\pi,$

where ε is $Sv-$ magnetic potential.

♣ *Optical antiferromagnetic $Sv-$ magnetic electromotive conformable $\Phi(\tau)$ microscale is presented*

$\mathcal{E}^{afr}_{\Phi(\tau)} = -\frac{d}{dt}\int_\tau \mathbb{I}_\sigma(-\epsilon^{4-4\sigma} - \varkappa^2\epsilon^{2-2\sigma} + (\epsilon^{1-\sigma}(\epsilon^{2-2\sigma}\mu + \epsilon^{1-\sigma}\frac{\partial\varkappa}{\partial\epsilon}) - \varkappa(\varkappa\epsilon^{1-\sigma}\mu + \epsilon^{1-2\sigma}(1-\sigma)))\mu\epsilon^{1-\sigma})d\pi.$

♣ *Optical antiferromagnetic $Sv-$optimistic conformable $\Phi(\tau)$ density is*

$\mathcal{D}^{afr}_{\Phi(\tau)} = (\epsilon^{1-\sigma}(\epsilon^{2-2\sigma}\mu + \epsilon^{1-\sigma}\frac{\partial\varkappa}{\partial\epsilon}) - \varkappa(\varkappa\epsilon^{1-\sigma}\mu + \epsilon^{1-2\sigma}(1-\sigma)))\mu\epsilon^{1-\sigma} - \varkappa^2\epsilon^{2-2\sigma} - \epsilon^{4-4\sigma}.$

♣ *Geometric antiferromagnetic $Sv-$ magnetic conformable $\Phi(\tau)$ microscale is presented by*

$\mathcal{M}^{afr}_{\Phi(\tau)} = \epsilon^{1-\sigma}\varepsilon\int_\tau \mathbb{I}_\sigma(-\varkappa^2\epsilon^{2-2\sigma} + (\epsilon^{1-\sigma}(\epsilon^{2-2\sigma}\mu + \epsilon^{1-\sigma}\frac{\partial\varkappa}{\partial\epsilon}) - \varkappa(\varkappa\epsilon^{1-\sigma}\mu + \epsilon^{1-2\sigma}(1-\sigma)))\mu\epsilon^{1-\sigma} - \epsilon^{4-4\sigma})d\pi.$

Fig. 1 shows the antiferromagnetic $Sv-$ optimistic conformable $\Phi(\tau)$ density in reactor domain along with fluid indicating the $Sv-$ magnetic potential.

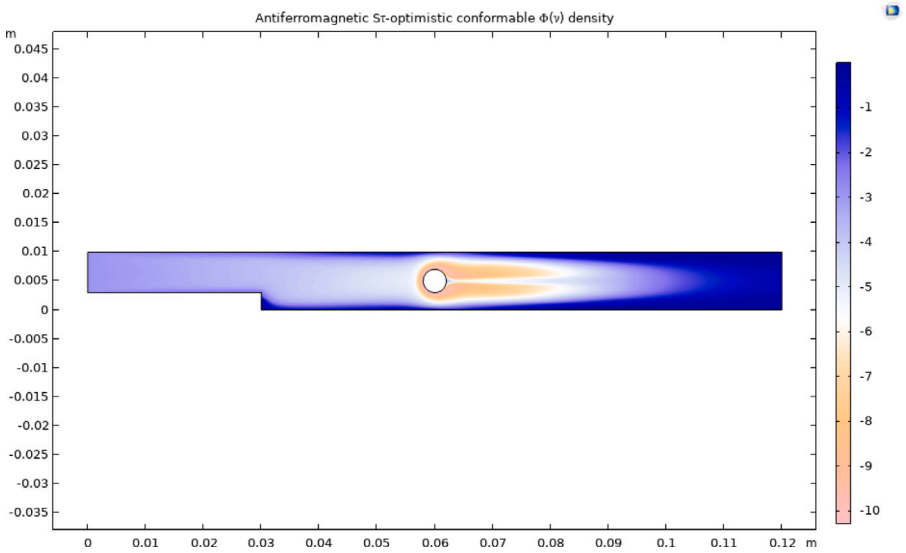

Fig. 2. $S\nu-$ optimistic conformable $\Phi(\nu)$ density with reactor at $200K$.

$S\nu-$Electromotive conformable $\Phi(\nu)$ microscale

First, we can represent by

$$\Phi(\nu) = \epsilon^{1-\sigma}\tau + \epsilon^{1-\sigma}\mu\beta.$$

By conformal differentiating above field, we get

$$\partial_\sigma \Phi(\nu) = \epsilon^{1-2\sigma}(1-\sigma)\tau + (\epsilon^{2-2\sigma}\mu^2 + \epsilon^{2-2\sigma})\nu + (\mu(1-\sigma)\epsilon^{-2\sigma+1} + \frac{\partial\mu}{\partial\epsilon}\epsilon^{2-2\sigma})\beta.$$

Therefore, we can write

$$\Phi(\nu)\times\partial_\sigma\Phi(\nu) = -\epsilon^{1-\sigma}\mu(\epsilon^{2-2\sigma}\mu^2 + \epsilon^{2-2\sigma})\tau + (\epsilon^{1-\sigma}(\mu(1$$
$$-\sigma)\epsilon^{-2\sigma+1} + \frac{\partial\mu}{\partial\epsilon}\epsilon^{2-2\sigma}) - \epsilon^{1-\sigma}\mu\epsilon^{1-2\sigma}(1-\sigma))\nu + \epsilon^{1-\sigma}(\epsilon^{2-2\sigma}\mu^2 + \epsilon^{2-2\sigma})\beta.$$

The flow of $\Phi(\tau)$ is written by

$$\partial_t\Phi(\nu) = -\epsilon^{2-2\sigma}\mu\mathcal{L}\tau + (\epsilon^{1-\sigma}\mathcal{F} + \epsilon^{1-\sigma}\mu(\epsilon^{1-\sigma}\frac{\partial\mathcal{L}}{\partial\epsilon}$$
$$+\mathcal{F}\epsilon^{1-\sigma}\mu))\nu + (\epsilon^{1-\sigma}\frac{\partial}{\partial t}(\mu) + \mathcal{L}\epsilon^{1-\sigma})\beta.$$

♣ *Optical $S\nu-$magnetic electromotive conformable $\Phi(\nu)$ microscale is presented*

$$\mathcal{E}_{\phi(\nu)} = -\frac{d}{dt}\int_\tau \mathbb{I}_\sigma(\epsilon^{1-\sigma}(\epsilon^{1-\sigma}\frac{\partial\mu}{\partial t} + \mathcal{L}\epsilon^{1-\sigma}) + \varkappa(\epsilon^{1-\sigma}\mathcal{F}$$
$$+\epsilon^{1-\sigma}\mu(\epsilon^{1-\sigma}\frac{\partial\mathcal{L}}{\partial\epsilon} + \mathcal{F}\epsilon^{1-\sigma}\mu)) - \epsilon^{3-3\sigma}\mu^2\mathcal{L})d\pi.$$

♣ *Optical $S\nu-$optimistic conformable $\Phi(\nu)$ density is*

$$\mathcal{D}_{\Phi(\nu)} = \varkappa(\epsilon^{1-\sigma}\mathcal{F} + \epsilon^{1-\sigma}\mu(\epsilon^{1-\sigma}\frac{\partial\mathcal{L}}{\partial\epsilon} + \mathcal{F}\epsilon^{1-\sigma}\mu))$$
$$-\epsilon^{3-3\sigma}\mu^2\mathcal{L} + \epsilon^{1-\sigma}(\epsilon^{1-\sigma}\frac{\partial\mu}{\partial t} + \mathcal{L}\epsilon^{1-\sigma}).$$

♣ *Geometric $S\nu-$magnetic conformable $\Phi(\nu)$ microscale is presented by*

$${}^B\mathcal{M}_{\Phi(\nu)} = \epsilon^{1-\sigma}\varepsilon\int_\tau \mathbb{I}_\sigma(-\epsilon^{3-3\sigma}\mu^2\mathcal{L} + \varkappa(\epsilon^{1-\sigma}\mathcal{F}$$
$$+\epsilon^{1-\sigma}\mu(\epsilon^{1-\sigma}\frac{\partial\mathcal{L}}{\partial\epsilon} + \mathcal{F}\epsilon^{1-\sigma}\mu)) + \epsilon^{1-\sigma}(\epsilon^{1-\sigma}\frac{\partial\mu}{\partial t} + \mathcal{L}\epsilon^{1-\sigma}))d\pi,$$

where ε is $S\nu-$ magnetic potential.

♣ *Optical antiferromagnetic $S\nu-$ magnetic electromotive conformable $\Phi(\nu)$ microscale is presented*

$$\mathcal{E}^{afr}_{\Phi(\nu)} = -\frac{d}{dt}\int_\tau \mathbb{I}_\sigma(\epsilon^{4-4\sigma}(\mu^2+1) - \epsilon^{2-2\sigma}\mu^2(\epsilon^{2-2\sigma}\mu^2 + \epsilon^{2-2\sigma})$$
$$+\varkappa(\epsilon^{1-\sigma}(\mu(1-\sigma)\epsilon^{-2\sigma+1} + \frac{\partial\mu}{\partial\epsilon}\epsilon^{2-2\sigma}) - \epsilon^{1-\sigma}\mu\epsilon^{1-2\sigma}(1-\sigma)))d\pi.$$

♣ *Optical antiferromagnetic $S\nu-$optimistic conformable $\Phi(\nu)$ density is*

$$\mathcal{D}^{afr}_{\Phi(\nu)} = -\epsilon^{2-2\sigma}\mu^2(\epsilon^{2-2\sigma}\mu^2 + \epsilon^{2-2\sigma}) + \varkappa(\epsilon^{1-\sigma}(\mu(1-\sigma)\epsilon^{-2\sigma+1}$$
$$+\frac{\partial\mu}{\partial\epsilon}\epsilon^{2-2\sigma}) - \epsilon^{1-\sigma}\mu\epsilon^{1-2\sigma}(1-\sigma)) + \epsilon^{2-2\sigma}(\epsilon^{2-2\sigma}\mu^2 + \epsilon^{2-2\sigma}).$$

♣ *Geometric antiferromagnetic $S\nu-$ magnetic conformable $\Phi(\nu)$ microscale is presented by*

$$\mathcal{M}^{afr}_{\Phi(\nu)} = \epsilon^{1-\sigma}\varepsilon\int_\tau \mathbb{I}_\sigma(\varkappa(\epsilon^{1-\sigma}(\mu(1-\sigma)\epsilon^{-2\sigma+1} + \frac{\partial\mu}{\partial\epsilon}\epsilon^{2-2\sigma}) - \epsilon^{1-\sigma}\mu\epsilon^{1-2\sigma}(1$$
$$-\sigma)) - \epsilon^{2-2\sigma}\mu^2(\epsilon^{2-2\sigma}\mu^2 + \epsilon^{2-2\sigma}) + \epsilon^{2-2\sigma}(\epsilon^{2-2\sigma}\mu^2 + \epsilon^{2-2\sigma}))d\pi.$$

Fig. 2 shows the antiferromagnetic $S\nu-$ optimistic conformable $\Phi(\nu)$ density in reactor domain along with fluid indicating the $S\nu-$ magnetic potential.

$S\nu-$Electromotive conformable $\Phi(\beta)$ microscale

First, we can represent by

$$\Phi(\beta) = -\varkappa\tau + \mu\epsilon^{1-\sigma}\nu.$$

By conformal differentiating above field, we get

$$\partial_\sigma\Phi(\beta) = (-\frac{\partial\varkappa}{\partial\epsilon}\epsilon^{1-\sigma} + \epsilon^{2-2\sigma}\mu)\tau + (\epsilon^{2-2\sigma}\frac{\partial\mu}{\partial\epsilon}$$
$$+(1-\sigma)\epsilon^{1-2\sigma}\mu - \epsilon^{1-\sigma}\varkappa)\nu + (\mu\epsilon^{1-\sigma})^2\beta.$$

Therefore, we can write

$$\Phi(\beta)\times\partial_\sigma\Phi(\beta) = \mu^3\epsilon^{3-3\sigma}\tau - \varkappa(\mu\epsilon^{1-\sigma})^2\nu - (\varkappa(\epsilon^{2-2\sigma}\frac{\partial\mu}{\partial\epsilon}$$
$$+(1-\sigma)\epsilon^{1-2\sigma}\mu - \epsilon^{1-\sigma}\varkappa) + \mu\epsilon^{1-\sigma}(-\frac{\partial\varkappa}{\partial\epsilon}\epsilon^{1-\sigma} + \epsilon^{2-2\sigma}\mu))\beta.$$

The flow of $\Phi(\beta)$ is written by

$$\partial_t\Phi(\beta) = (\mu\mathcal{F}\epsilon^{2-2\sigma} - \frac{\partial\varkappa}{\partial t})\tau + (\frac{\partial\mu}{\partial t}\epsilon^{1-\sigma}$$
$$-\varkappa\mathcal{F})\nu + (\mu\epsilon^{1-\sigma}(\frac{\partial\mathcal{L}}{\partial\epsilon}\epsilon^{1-\sigma} + \mathcal{F}\epsilon^{1-\sigma}\mu) - \varkappa\mathcal{L})\beta.$$

♣ *Optical $S\nu-$magnetic electromotive conformable $\Phi(\beta)$ microscale is presented*

$$\mathcal{E}_{\Phi(\beta)} = -\frac{d}{dt}\int_\tau \mathbb{I}_\sigma(\mu\epsilon^{1-\sigma}(\mu\mathcal{F}\epsilon^{2-2\sigma} - \frac{\partial\varkappa}{\partial t}) + (\frac{\partial\mu}{\partial t}\epsilon^{1-\sigma}$$
$$-\varkappa\mathcal{F})\varkappa - (\mu\epsilon^{1-\sigma}(\frac{\partial\mathcal{L}}{\partial\epsilon}\epsilon^{1-\sigma} + \mathcal{F}\epsilon^{1-\sigma}\mu) - \varkappa\mathcal{L})\epsilon^{1-\sigma})d\pi.$$

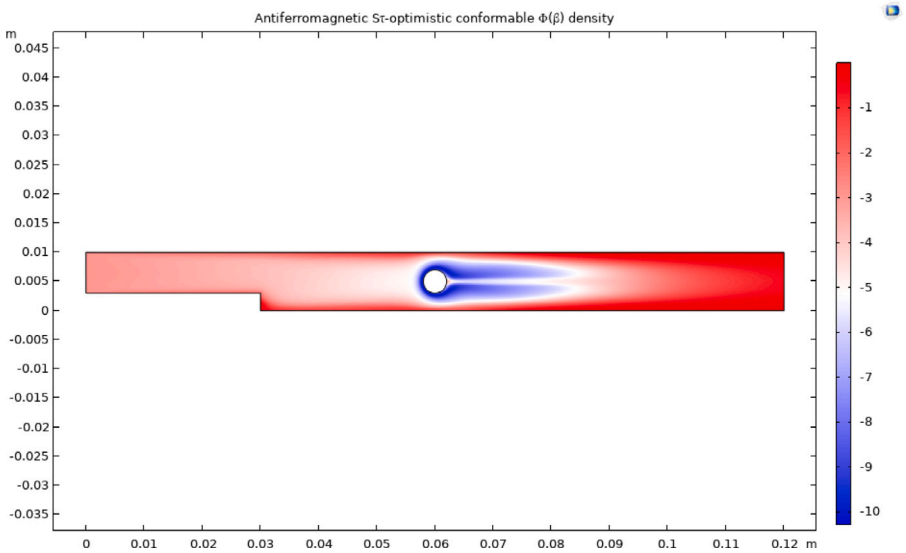

Fig. 3. $Sv-$ optimistic conformable $\Phi(\beta)$ density with reactor at $400K$.

♣ *Optical* $Sv-$*optimistic conformable* $\Phi(\beta)$ *density is*

$$D_{\Phi(\beta)} = (\frac{\partial \mu}{\partial t}\epsilon^{1-\sigma} - \varkappa\mathcal{F})\varkappa + \epsilon^{1-\sigma}\mu(\mu\mathcal{F}\epsilon^{2-2\sigma} - \frac{\partial \varkappa}{\partial t}) - (\mu\epsilon^{1-\sigma}(\frac{\partial \mathcal{L}}{\partial \epsilon}\epsilon^{1-\sigma} + \mathcal{F}\epsilon^{1-\sigma}\mu) - \varkappa\mathcal{L})\epsilon^{1-\sigma}.$$

♣ *Geometric* $Sv-$*magnetic conformable* $\Phi(\beta)$ *microscale is presented by*

$${}^{B}\mathcal{M}_{\Phi(\beta)} = \epsilon^{1-\sigma}\varepsilon \int_{\tau} \mathbb{I}_{\sigma}(-\epsilon^{1-\sigma}(\mu\epsilon^{1-\sigma}(\frac{\partial \mathcal{L}}{\partial \epsilon}\epsilon^{1-\sigma} + \mathcal{F}\epsilon^{1-\sigma}\mu) - \varkappa\mathcal{L}) + (\frac{\partial \mu}{\partial t}\epsilon^{1-\sigma} - \varkappa\mathcal{F})\varkappa + \epsilon^{1-\sigma}\mu(\mu\mathcal{F}\epsilon^{2-2\sigma} - \frac{\partial \varkappa}{\partial t}))d\pi,$$

where ε *is* $Sv-$ *magnetic potential.*

♣ *Optical antiferromagnetic* $Sv-$ *magnetic electromotive conformable* $\Phi(\beta)$ *microscale is presented*

$$\mathcal{E}^{afr}_{\Phi(\beta)} = -\frac{d}{dt}\int_{\tau} \mathbb{I}_{\sigma}(\mu^4\epsilon^{4-4\sigma} - \varkappa^2(\mu\epsilon^{1-\sigma})^2 + \epsilon^{1-\sigma}(\varkappa(\epsilon^{2-2\sigma}\frac{\partial \mu}{\partial \epsilon} + (1-\sigma)\epsilon^{1-2\sigma}\mu - \epsilon^{1-\sigma}\varkappa) + \mu\epsilon^{1-\sigma}(-\frac{\partial \varkappa}{\partial \epsilon}\epsilon^{1-\sigma} + \epsilon^{2-2\sigma}\mu)))d\pi.$$

♣ *Optical antiferromagnetic* $Sv-$*optimistic conformable* $\Phi(\beta)$ *density is*

$$D^{afr}_{\Phi(\beta)} = \mu^4\epsilon^{4-4\sigma} - \varkappa^2(\mu\epsilon^{1-\sigma})^2 + \epsilon^{1-\sigma}(\varkappa(\epsilon^{2-2\sigma}\frac{\partial \mu}{\partial \epsilon} + (1-\sigma)\epsilon^{1-2\sigma}\mu - \epsilon^{1-\sigma}\varkappa) + \mu\epsilon^{1-\sigma}(-\frac{\partial \varkappa}{\partial \epsilon}\epsilon^{1-\sigma} + \epsilon^{2-2\sigma}\mu)).$$

♣ *Geometric antiferromagnetic* $Sv-$ *magnetic conformable* $\Phi(\beta)$ *microscale is presented by*

$$\mathcal{M}^{afr}_{\Phi(\beta)} = \epsilon^{1-\sigma}\varepsilon \int_{\tau} \mathbb{I}_{\sigma}(-\varkappa^2(\mu\epsilon^{1-\sigma})^2 + \epsilon^{1-\sigma}(\varkappa(\epsilon^{2-2\sigma}\frac{\partial \mu}{\partial \epsilon} + (1-\sigma)\epsilon^{1-2\sigma}\mu - \epsilon^{1-\sigma}\varkappa) + \mu\epsilon^{1-\sigma}(-\frac{\partial \varkappa}{\partial \epsilon}\epsilon^{1-\sigma} + \epsilon^{2-2\sigma}\mu)) + \mu^4\epsilon^{4-4\sigma})d\pi.$$

Fig. 3 shows the antiferromagnetic $Sv-$ optimistic conformable $\Phi(\beta)$ density in reactor domain along with fluid indicating the $Sv-$ magnetic potential.

Conclusion

Spherical optical electromagnetic energy and flux are illustrated by flexible elastic curves, optical waves and biharmonic sonics. The results of optical modeling of biharmonic magnetic curves with optical applications are characterized.

In this article, we present spherical antiferromagnetic $Sv-$magnetic electromotive conformable $\Phi(\tau), \Phi(\nu), \Phi(\beta)$ microscales in conformable deSitter space. Also, we get optical antiferromagnetic $Sv-$ optimistic conformable $\Phi(\tau), \Phi(\nu), \Phi(\beta)$ densities. Finally, we obtain geometric antiferromagnetic $Sv-$magnetic conformable $\Phi(\tau), \Phi(\nu), \Phi(\beta)$ microscales in conformable deSitter space.

CRediT authorship contribution statement

Ferdous M. Tawfig: Investigation, Data curation, Conceptualization. **Talat Körpinar:** Visualization, Validation, Supervision, Funding acquisition, Conceptualization. **Zeliha Körpinar:** Writing – review & editing, Writing – original draft, Visualization, Validation, Supervision, Methodology, Investigation. **Mustafa Inc:** Resources, Project administration, Methodology, Formal analysis.

Declaration of competing interest

I am the corresponding author and on behalf of all authors I declare that we have no known competing financial interests or personal relationships that could have appeared to influence the work reported in this paper.

Data availability

No data was used for the research described in the article.

Acknowledgments

This research was supported by the Researchers Supporting Project Number (RSP2024R440), King Saud University, Riyadh, Saudi Arabia.

References

[1] Gu H, Duits MH, Mugele F. Droplets formation and merging in two-phase flow microfluidics. Int J Mol Sci 2011;12(4):2572–97.
[2] Pit AM, Duits MH, Mugele F. Droplet manipulations in two phase flow microfluidics. Micromachines 2015;6(11):1768–93.
[3] Zhao CX, Middelberg AP. Two-phase microfluidic flows. Chem Eng Sci 2011;66(7):1394–411.
[4] Tao G, Stolyarov AM, Abouraddy AF. Multi-material fibers. Int J Appl Glass Sci 2012;3:349.
[5] Sattari A, Hanafizadeh P, Hoorfar M. Multiphase flow in microfluidics: From droplets and bubbles to the encapsulated structures. Adv Colloid Interface Sci 2020;282:102208.
[6] Fink Y, Winn J, Fan S, Chen C, Michel J, Joannopoulos J, Thomas E. A dielectric omnidirectional reflector. Science 1998;282:1679.

[7] Korpinar T, Körpınar Z. Timelike spherical magnetic $\mathbb{S}_{\beta}$ flux flows with heisenberg sphericalferromagnetic spin with some solutions. Optik 2021;242:166745.
[8] Körpınar Z, Korpinar T. Optical spherical electromotive density with some fractional applications with Laplace transform in spherical Heisenberg space $\mathbb{S}^2_{\mathbb{H}}$. Optik 2021;245:167596.
[9] Körpınar T. Optical electromotive force with Heisenberg spherical ferromagnetic spin. Optik 2021;245:167521.
[10] Körpınar Z, Korpinar T. Optical hybrid electric and magnetic $\mathbf{B}_1$-phase with Landau Lifshitz approach. Optik 2021;247:167917.
[11] Garcia de Andrade LC. Non-Riemannian geometry of twisted flux tubes. Braz J Phys 2006;36(4A):1290–5.
[12] Garcia de Andrade LC. Riemannian geometry of twisted magnetic flux tubes in almost helical plasma flows. Phys Plasmas 2006;13(2):022309-022309.
[13] Garcia de Andrade LC. Vortex filaments in MHD. Phys Scr 2006;73(5):484.
[14] Guo B, Ding S. Landau-lifshitz equations. World Scientific; 2008.
[15] Vieira VR, Horley PP. The Frenet–Serret representation of the Landau–Lifshitz–Gilbert equation. J Phys A 2012;45(6):065208.
[16] Hasimoto H. A soliton on a vortex filament. J Fluid Mech 1972;51(3):477–85.
[17] Jones RC. A new calculus for the treatment of optical systems I. Description and discussion of the calculus. J Opt Soc Amer 1941;31:488–93.
[18] Berry MV, Klein S. Geometric phases from stacks of crystal plates. J Modern Opt 1996;43:165–80.
[19] Biener G, Niv A, Kleiner V, Hasman E. Formation of helical beams by use of Pancharatnam–Berry phase optical elements. Opt Lett 2002;27:1875–7.
[20] Zygelman B. Appearance of gauge potentials in atomic collision physics. Phys Lett A 1987;125:476–81.
[21] Smit J. The spontaneous hall effect in ferromagnetics I. Physica 1955;21:877.
[22] Son DT, Yamamoto N. Berry curvature, triangle anomalies, and the chiral magnetic effect in Fermi liquids. Phys Rev Lett 2012;109:81602.
[23] Körpınar T, Demirkol RC. Electromagnetic curves of the linearly polarized light wave along an optical fiber in a 3D semi-Riemannian manifold. J Modern Opt 2019;66(8):857–67.
[24] Körpınar T, Demirkol RC, Körpınar Z. Soliton propagation of electromagnetic field vectors of polarized light ray traveling in a coiled optical fiber in Minkowski space with Bishop equations. Eur Phys J D 2019;73:203.
[25] Körpınar T, Demirkol RC, Körpınar Z. Soliton propagation of electromagnetic field vectors of polarized light ray traveling in a coiled optical fiber in the ordinary space. Int J Geom Methods Mod Phys 2019;16(8):1950117.
[26] Körpınar T, Demirkol RC, Körpınar Z. Soliton propagation of electromagnetic field vectors of polarized light ray traveling along with coiled optical fiber on the unit 2-sphere S^2. Rev Mexicana Fís 2019;65:626.
[27] Körpınar T, Demirkol RC. Electromagnetic curves of the linearly polarized light wave along an optical fiber in a 3D Riemannian manifold with Bishop equations. Optik 2020;200:163334.
[28] Cao Q, Li Z, Wang Z, Han X. Rotational motion and lateral migration of an elliptical magnetic particle in a microchannel under a uniform magnetic field. Microfluid Nanofluid 2018;22:3.
[29] Cao Q, Liu M, Wang Z, Han X, Li L. Dynamic motion analysis of magnetic particles in microfluidic systems under an external gradient magnetic field. Microfluid Nanofluid 2017;21(2):24.
[30] Erb RM, Martin JJ, Soheilian R, Pan C, Barber JR. Actuating soft matter with magnetic torque. Adv Funct Mater 2016;26(22):3859–80.
[31] Furlani EP, Ng KC. Analytical model of magnetic nanoparticle capture in the microvasculature. Phys Rev E 2006;73(6):061919.
[32] Körpınar T, Demirkol RC, Körpınar Z, Asil V. Maxwellian evolution equations along the uniform optical fiber in Minkowski space. Rev Mex Fis 2020;66(4):431.
[33] Körpınar T, Demirkol RC, Körpınar Z, Asil V. Maxwellian evolution equations along the uniform optical fiber in Minkowski space. Optik 2020;217:164561.
[34] Tomita A, Chiao Y. Observation of Berry's topological phase by use of an optical fiber. Phys Rev Lett 1986;57:937.
[35] Wassmann F, Ankiewicz A. Berry's phase analysis of polarization rotation in helicoidal fibers. Appl Opt 1998;37:3902.
[36] Balakrishnan R, Bishop R, Dandoloff R. Geometric phase in the classical continuous antiferromagnetic Heisenberg spin chain. Phys Rev Lett 1990;64:2107.
[37] Balakrishnan R, Bishop R, Dandoloff R. Anholonomy of a moving space curve and applications to classical magnetic chains. Phys Rev B 1993;47:3108.
[38] Balakrishnan R, Dandoloff R. The Schrodinger equation as a moving curve. Phys Lett A 1999;260:62.
[39] Körpinar T, Demirkol RC. Frictional magnetic curves in 3D Riemannian manifolds. Int J Geom Methods Mod Phys 2018;15:1850020.
[40] Körpinar T, Demirkol RC. Gravitational magnetic curves on 3D Riemannian manifolds. Int J Geom Methods Mod Phys 2018;15:1850184.
[41] Körpinar T. Optical directional binormal magnetic flows with geometric phase: Heisenberg ferromagnetic model. Opt Int J Light Electron Opt 2020;219:165134.
[42] Kugler M, Shtrikman S. Berry's phase, locally inertial frames, and classical analogues. Phys Rev D 1988;37(4):934.
[43] Dandoloff R, Zakrzewski WJ. Parallel transport along a space curve and related phases. J Phys A: Math Gen 1989;22(11):L461.
[44] Satija II, Balakrishan R. Geometric phases in twisted strips. Phys Lett A 2009;373(39):3582.
[45] Yamashita O. Effect of the geometrical phase shift on the spin and orbital angular momenta of light traveling in a coiled optical fiber with optical activity. Opt Commun 2012;285:3740.
[46] Yamashita O. Geometrical phase shift of the extrinsic orbital angular momentum density of light propagating in a helically wound optical fiber. Opt Commun 2012;285:3061.
[47] Lamb GL. Solitons on moving space curves. J Math Phys 1977;18:1654.
[48] Murugesh S, Balakrishnan R. New connections between moving curves and soliton equations. Phys Lett A 2001;290:81.
[49] Gürbüz N. The differantial formula of hasimoto transformation in Minkowski 3-space. Int J Math Math Sci 2005;2005:542381.
[50] Körpınar Z, Körpınar T. Optical hybrid electric and magnetic B_1-phase with Landau Lifshitz approach. Optik 2021;247:167917.
[51] Körpınar T, Körpınar Z, Yeneroğlu M. Optical energy of spherical velocity with optical magnetic density in heisenberg sphere space $\mathbb{S}^2_{Heis^3}$. Optik 2021;247:167937.
[52] Körpınar T, Sazak A, Körpınar Z. Optical effects of some motion equations on quasi-frame with compatible Hasimoto map. Optik 2021;247:167914.
[53] Körpınar Z, Körpınar T. Optical tangent hybrid electromotives for tangent hybrid magnetic particle. Optik 2021;247:167823.
[54] Körpınar T, Körpınar Z, Asil V. New approach for optical electroostimistic phase with optical quasi potential energy. Optik 2022;251:168291.
[55] Körpınar T, Ünlütürk Y, Körpınar Z. A new version of the motion equations of pseudo null curves with compatible Hasimoto map. Opt Quantum Electron 2023;55(1):23.
[56] Körpınar T, Körpınar Z, Demirkol RC. Binormal schrodinger system of wave propagation field of light radiate in the normal direction with q-HATM approach. Optik 2020;235:166444.
[57] Inc M, Korpinar T, Korpinar Z. Spherical traveling wave hypothesis for geometric optical phase with speherical magnetic ferromagnetic system. Opt Quantum Electron 2023;55(2):127.
[58] Zhu L, Luo D, Liu Y. Effect of the nano/microscale structure of biomaterial scaffolds on bone regeneration. Int J Oral Sci 2020;12(1):6.
[59] Körpinar T, Körpinar Z. New modeling for Heisenberg velocity microfluidic of optical ferromagnetic mKdV flux. Opt Quantum Electron 2023;55(6):523.
[60] Ghayesh MH, Farajpour A. A review on the mechanics of functionally graded nanoscale and microscale structures. Internat J Engrg Sci 2019;137:8–36.
[61] Körpinar T, Demirkol RC, Körpinar Z. On the new conformable optical ferromagnetic and antiferromagnetic magnetically driven waves. Opt Quantum Electron 2023;55(6):496.
[62] Xiong T, Zhang K, Jiang Y, Yu P, Mao L. Ion current rectification: from nanoscale to microscale. Sci China Chem 2019;62:1346–59.
[63] Körpinar T, Körpinar Z. Antiferromagnetic complex electromotive microscale with first type Schrödinger frame. Opt Quantum Electron 2023;55(6):505.
[64] Jiao H, Yang W, Ruan ZE, Yu J, Liu J, Yang Y. Microscale mechanism of tailing thickening in metal mines. Int J Miner Metall Mater 2023;30(8):1538–47.
[65] Ashkin A, Dziedzic JM, Bjorkholm JE, Chu S. Observation of a single-beam gradient force optical trap for dielectric particles. Opt Lett 1986;11:288–90.
[66] Farquhar ME, Burrage K, Lawson BA. Robust graph-based upscaling of microscale fibrotic structures. In: 2021 computing in cardiology. cinC, Vol. 48, IEEE; 2021, p. 1–4.
[67] Dholakia K, Zemánek P. Colloquium: gripped by light: optical binding. Rev Modern Phys 2010;82:1767–91.
[68] Sultana J. Gravitational light bending in Weyl gravity and Schwarzschild-de Sitter spacetime. Symmetry 2024;16(1):101.
[69] Narayan K. de Sitter space and extremal surfaces for spheres. Phys Lett B 2016;753:308–14.
[70] Balasubramanian V, de Boer J, Minic D. Exploring de Sitter space and holography. Ann Phys 2003;303(1):59–116.
[71] Neupane I. Simple cosmological de Sitter solutions on spaces. Classical Quantum Gravity 2010;27(4):045011.
[72] Kavitha L, Parasuraman E, Gopi D, Bhuvaneswari S. Propagation of electromagnetic solitons in an antiferromagnetic spinladder medium. J Electromagn Waves Appl 2016;30(6):740–66.
[73] Sharaevskaya AY, Kalyabin DV, Beginin EN, Fetisov YK, Nikitov SA. Surface spin waves in coupled easy-axis antiferromagnetic films. J Magn Magn Mater 2019;475:778–81.
[74] Zhang YH, Sachdev S. Deconfined criticality and ghost Fermi surfaces at the onset of antiferromagnetism in a metal. Phys Rev B 2020;102(15):155124.